Motif distributions in phase-space networks for characterizing experimental two-phase flow patterns with chaotic features

Zhong-Ke Gao,[1,2] Ning-De Jin,[1] Wen-Xu Wang,[2] and Ying-Cheng Lai[2,3]
[1]*School of Electrical Engineering and Automation, Tianjin University, Tianjin 300072, China*
[2]*School of Electrical, Computer and Energy Engineering, Arizona State University, Tempe, Arizona 85287, USA*
[3]*Department of Physics, Arizona State University, Tempe, Arizona 85287, USA*
(Received 15 March 2010; published 16 July 2010)

The dynamics of two-phase flows have been a challenging problem in nonlinear dynamics and fluid mechanics. We propose a method to characterize and distinguish patterns from inclined water-oil flow experiments based on the concept of network motifs that have found great usage in network science and systems biology. In particular, we construct from measured time series phase-space complex networks and then calculate the distribution of a set of distinct network motifs. To gain insight, we first test the approach using time series from classical chaotic systems and find a universal feature: motif distributions from different chaotic systems are generally highly heterogeneous. Our main finding is that the distributions from experimental two-phase flows tend to be heterogeneous as well, suggesting the underlying chaotic nature of the flow patterns. Calculation of the maximal Lyapunov exponent provides further support for this. Motif distributions can thus be a feasible tool to understand the dynamics of realistic two-phase flow patterns.

DOI: 10.1103/PhysRevE.82.016210 PACS number(s): 05.45.Tp, 47.55.Ca, 89.75.Fb

I. INTRODUCTION

Oil-water two-phase flow is commonly observed in well bores, and its behaviors under a wide range of flow conditions and inclination angles constitute an outstanding interdisciplinary problem with significant applications to the petroleum industry. Understanding the dynamics of flow patterns is crucial to important problems such as predicting the pressure drop in inclined oil wells. Due to the interplay among many complex factors such as fluid turbulence, phase interfacial interaction, local relative movements between phases, and the existence of a gravitational component normal to the flow direction, an inclined oil-water flow exhibits highly irregular, random, and unsteady flow structure as compared with a vertical two-phase flow.

Earlier investigations of inclined oil-water two-phase flow were mainly focused on experimental observations. For example, Hill and Oolman [1] observed, in a 152-mm-inner-diameter (ID) pipe, a kind of segregated flow patterns where the water phase exists in most of the pipe but the flow tends to reverse near the bottom of the pipe. They observed that a small change in the deviation angle can cause a large change in the velocity profile distribution. Vigneaux *et al.* [2] measured the inclined oil-water flows in a 200-mm-ID pipe by using a high-frequency impedance probe and observed the occurrence of two main flow patterns: dispersed oil in water-pseudoslug (PS) flow and in water-countercurrent (CT) flow. Flores *et al.* [3] conducted a comprehensive experimental study of vertical and inclined oil-water flows with a 50.8-mm-ID pipe, and classified seven flow patterns in inclined oil-water flows with four water-dominated, two oil-dominated, and a transitional flow (TF) pattern.

In the 1990s, numerical simulation methods began to be widely used in the study of inclined oil-water flows. For example, Mobbs and Lucas [4] proposed, for inclined liquid-liquid flow, a large-amplitude turbulence model that incorporates qualitatively Kelvin-Helmholtz eddy characteristics. They found that the eddies grow and collapse periodically and their amplitudes can reach the value of the pipe diameter. Lucas [5] proposed a mathematical model of velocity profile for inclined oil-water flows, where predictions of local velocities agree with experiments but only for the upper and central parts of the pipe. Lucas and Jin [6,7] studied a drift-velocity model and homogeneous velocity measurement in inclined oil-water pipe flows, and demonstrated that the phase-distribution parameter and single-droplet terminal rise velocity can be greatly affected by inclination angles.

Despite the existing results, significant challenges in the study of oil-water two-phase flow remain. For example, detecting transitional flow is still an unsolved problem. Due to the complexity of the problem, analytical approaches are usually infeasible. The approach of nonlinear time series analysis [8] also has severe limitations as applied to oil-water two-phase flows, mainly due to the occurrence of CT flow pattern triggered by the gravitational component normal to the flow direction. In particular, in Ref. [9]. we pointed out that, although dispersion oil-in-water PS and CT flows can be distinguished by the methods of recurrence plot [10,11] and attractor-geometry morphological mapping [12], these methods appear to be ineffective for transitional flows. So far there has been no satisfactory understanding of the underlying dynamics leading to the formation and governing the evolution of patterns in such flows.

Quite recently, the approach of complex networks has been introduced into the study of two-phase flows [13], inspired by the general approach [14–21] of mapping time series to complex networks which are capable of characterizing many types of systems in nature and technology that contain a large number of components interacting with each other in a complicated manner [22–29]. In particular, in Ref. [14], Zhang and Small found that noisy periodic signals correspond to random networks and chaotic time series tend to generate small-world and scale-free network features. Bridging time series analysis and complex networks can be an

appealing approach for experimental data analysis and pattern recognition. Based on experimental measured time series from a two-phase flow, an artificial network can be constructed. Global features of the network, such as the degree distribution and community structures, can then be exploited to characterize the dynamical states of the flow [13]. The global characterization, however, totally ignores any local structural properties of the reconstructed network, which may contain important information about the underlying dynamics. It is thus of interest to develop an approach taking into account local structures in the reconstructed network.

In this paper, we exploit the concept of network motifs [30,31] to characterize two-phase flow patterns. Network motifs have been found to be fundamental to gene regulatory networks in systems biology [32] and are also useful for characterizing networks from other disciplines [17,33,34]. Our study is inspired by Ref. [17] which reported that distributions of subgraphs in complex networks transformed from time series can characterize and distinguish different types of continuous dynamics such as periodic, chaotic, and noisy periodic dynamics. Here, we develop a different network construction approach and apply it to experimental two-phase flows to identify different flow patterns in terms of motif distributions. Specifically, given a set of time series from a two-phase flow, typically conductance fluctuating signals from some inclined oil-water two-phase flow experiment, our first step is to reconstruct phase-space complex networks (PSCNs) using the general method developed in Ref. [35]. We then search for possible motifs from the reconstructed network and calculate their distributions. Our main result is that motif distributions do exist in the reconstructed networks and, strikingly, they tend to be highly heterogeneous, a feature that has been found to be common for PSCNs constructed from low-dimensional deterministic chaotic systems. The motif distribution can thus faithfully represent the distinct dynamical states of the two-phase flow. For example, when a transition in the flow pattern occurs, a characteristic change in the motif distribution arises. Our results suggest that motif distribution can potentially be a powerful tool for revealing the nonlinear dynamics of two-phase flows.

In Sec. II, we outline the basic procedure of reconstructing PSCNs from measured time series and illustrate how network motif distribution can be obtained to characterize typical deterministic chaotic systems. In Sec. III, we describe our inclined oil-water experimental flow loop facility and data acquisition method. We then construct PSCNs from conductance fluctuating signals and demonstrate that motif distributions are heterogeneous and can be used to distinguish flow patterns in different dynamical regimes. In Sec. V, we present conclusions.

II. RECONSTRUCTION OF PHASE-SPACE COMPLEX NETWORKS FROM TIME SERIES AND MOTIF DISTRIBUTIONS

Our method [13,35] to construct a complex network from measured time series can be described as follows. Given a time series $z(it)$ $(i=1,2,\ldots,M)$, where t is the sampling interval and M is the sample size, we construct a sequence of phase-space vectors according to the standard delay-coordinate embedding method [36–38],

$$\begin{aligned}\vec{X} &= \{x_k(1), x_k(2), \ldots, x_k(m)\} \\ &= \{z(kt), z(kt+\tau), \ldots, z(kt+[m-1]\tau)\},\end{aligned} \tag{1}$$

where τ is the delay time, m is the embedding dimension, $k=1,2,\ldots,N$, and $N=M-(m-1)\tau/t$ is the total number of vector points in the reconstructed phase space. There are various empirical criteria for choosing the delay time τ, and we have used a correlation-integral-based method (see, e.g., Ref. [39]) for this purpose. For the choice of the embedding dimension, there exists a rigorous mathematical criterion [36,38]. For noisy time series it is convenient to use some heuristic criterion such as the one based on distinguishing false nearest neighbors (FNNs) [40] in the reconstructed phase space. The FNN method can generate a minimum embedding dimension m that ensures unfolding of orbits in the phase space, so that there are no false nearest neighbors for every orbit point. In contrast, if the embedding dimension is less than m, orbits in the phase space cannot be fully unfolded. After m is determined, we employ the correlation-integral-based algorithm [39] to determine τ. We note that if τ is too small, the reconstructed attractor can be compressed along the identity line and, if τ is too large, trajectories on the attractor may become disconnected. Our choice of τ avoids these undesirable situations.

To construct a network, we regard each vector point as a node and use the phase-space distance to determine the edges. Given two vector points $\vec{X}_i$ and $\vec{X}_j$, the phase-space distance is defined to be

$$d_{ij} = \sum_{n=1}^{m} \|X_i(n) - X_j(n)\|, \tag{2}$$

where $X_i(n)=z[i+(n-1)\tau]$ is the nth element of $\vec{X}_i$. This generates, for all nodes (vector points) in the network, a distance matrix $\mathbf{D}=(d_{ij})$. By choosing a proper threshold value r_c, where a distance is regarded as one or zero if it is greater than or less than r_c, respectively, we obtain the adjacency matrix $\mathbf{A}=(a_{ij})$,

$$A_{ij} = \begin{cases} 1, & \text{if} |d_{ij}| \le r_c \\ 0, & \text{if} |d_{ij}| > r_c. \end{cases} \tag{3}$$

Thus, an edge connecting node i and j exists if $|d_{ij}| \le r_c$, while there is no edge between i and j if $|d_{ij}| > r_c$. The topology of the reconstructed PSCN is determined entirely by $\mathbf{A}$.

A key issue in extracting network from deterministic chaotic time series is then the choice of the threshold r_c. In this regard, the method of choosing the threshold presented in Ref. [35] is effective for small-size networks. For large networks, the method can result in unrealistic values of the threshold, leading possibly to loss of information about the local phase-space or motif structure. Take, for example, networks reconstructed from chaotic systems. We are interested in exploring the interplay between network motifs and the fundamental building blocks of chaotic set: unstable periodic

orbits (UPOs). In order for UPOs to be represented adequately, the measured time series need to be long, resulting in large phase-space networks. In particular, for a chaotic attractor, a typical trajectory tends to approach different UPOs in different times, which constitute the "skeleton" of the attractor. In the network representation, the UPOs are effectively motifs that determine the cluster structure of the network. In order to represent the cluster structure, it is necessary that the reconstructed trajectory approach different UPOs a number of times. It is thus useful to choose a somewhat larger threshold: we choose r_c to be about 18–20 % of the root-mean-square (rms) value of the measured signal. It should be noted that in a recent method [17], for each phase-space point (node), a fixed number of nearest neighbors are chosen for defining connections. Our approach is different in that we use a fixed threshold to construct networks for flows of different patterns.

To illustrate the structure of PSCNs from typical chaotic systems, we consider three classical examples: (1) chaotic Lorenz system [41] given by $\dot{x}=16(y-x)$, $\dot{y}=x(45.92-z)-y$, and $\dot{z}=xy-4z$; (2) driven Duffing oscillator described by $\dot{x}=y$, $\dot{y}=-0.05y+0.5x-0.5x^3+7.5\cos(z)$, and $\dot{z}=1$; and (3) chaotic Rössler oscillator [42] defined by $\dot{x}=-y-x$, $\dot{y}=x+0.2y$, and $\dot{z}=0.2+(x-5.7)z$. To visualize the PSCNs, we use the Kamada-Kawai spring embedding algorithm [43]. The results are shown in Fig. 1. For each example, we observe some resemblance between the PSCN and the original chaotic attractor. After PSCNs are obtained, we employ the software FANMOD to detect network motifs. The software is developed using the Wernicke algorithm proposed in Refs. [44,45]. To be concrete, we focus on six different motifs of size four (i.e., four nodes) and calculate their frequencies of occurrence, as shown in Fig. 2. We observe a common feature among three examples: the motif distribution is highly heterogeneous. For example, the frequencies of motifs A and B are apparently much higher than those of others (e.g., motifs E and F). The heterogeneity originates from the UPOs embedded in the chaotic attractor. It has been known that, while the infinite set of periodic orbits embedded in a chaotic set are all unstable, their stabilities as determined by the corresponding largest eigenvalues are typically quite heterogeneous. In fact, a small set of UPOs can be significantly less unstable than the others. In the phase space, a UPO appears as a closed loop. A chaotic trajectory tends to spend substantially more time near weakly unstable orbits. As a result, there can be many recurrences near such a UPO, giving rise to a cluster in the corresponding PSCN, as can be seen from Fig. 1 and 2. We have also tested numerically that the motif distributions are robust with respect to variation in the network size, insofar as there are at least a few thousands of nodes.

Will weak noise affect the heterogeneous nature in the motif distribution of PSCN from chaotic time series? To address this question, we add Gaussian white noise to the chaotic Rössler time series to generate two time series whose signal-to-noise ratios (SNRs) are 20 and 10 dB, respectively. We find that, for SNR=20 dB, the network structure and motif distribution are essentially the same, as shown in Fig. 3(a). In particular, the strong heterogeneity in the motif distribution and the existence of motifs E and F are unchanged.

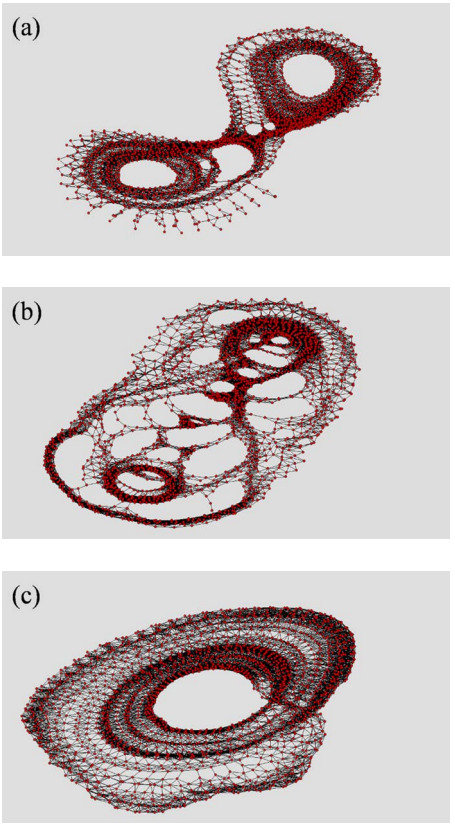

FIG. 1. (Color online) PSCN of 2000 nodes from (a) Lorenz system with $m=3$, $\tau=6$, $r_c=2.285$, and $t=20$; (b) Duffing system with $m=3$, $\tau=7$, $r_c=0.439$, and $t=100$; and (c) Rössler system with $m=3$, $\tau=7$, $r_c=1.176$, and $t=200$. The resulting networks are drawn by the software UCINET and PAJEK [46,47].

For larger noise amplitude, i.e., SNR=10 dB, distortion in the network structure arises, as shown in Fig. 3(b), but the feature of heterogeneity still remains. It is noteworthy that the presence of noise tends to suppress the heterogeneity of motif distributions in PSCNs for chaotic systems, as demonstrated in Fig. 3(b). In particular, under noise an unstable periodic orbit may not close on itself and the transitions

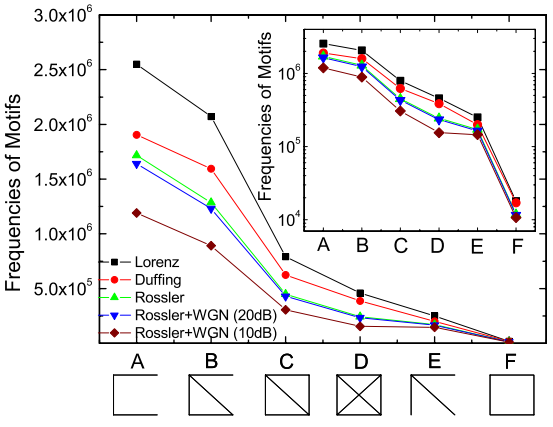

FIG. 2. (Color online) Motif distributions from the three chaotic PSCNs in Fig. 1. The inset shows the motif distributions on logarithmic scale.

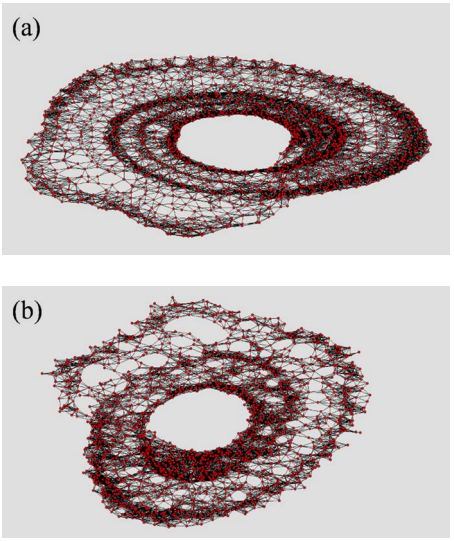

FIG. 3. (Color online) PSCN of 2000 nodes from Rössler chaotic time series corrupted by Gaussian white noise. (a) SNR =20 dB and (b) SNR=10 dB.

among different orbits are randomized. The distribution of all motifs will be influenced by the randomization but, statistically, the motifs with higher frequencies are influenced more than those with lower frequencies. This can be understood by noting that the distortions to individual motifs occur with approximately the same probabilities, regardless of the motif type. As a result, the motif with the highest frequency (motif A) is much more sensitive to noise than other motifs, reducing considerably its absolute number. Despite this effect under strong noise, for weak noise, the heterogeneous distribution of motifs appears to be robust, which can then be used as a fingerprint for distinguishing chaotic time series.

In addition, we note that the ranking of six motifs for chaotic time series is in agreement with that in Ref. [17], except for the reverse order between motifs D and E. This similarity illuminates that most motifs are insensitive to the definitions of connections among nodes in the phase space, either by fixing the number of nearest neighbors [17] or by the current distance threshold. Nevertheless, the connecting scheme plays an important role in the frequencies of motifs D and E, which can be used as a criterion for classifying different dynamics [17]. However, the intensities of heterogeneity in motif distributions for different chaotic time series are distinctly different from our method. In this regard, our approach complements the approach in Ref. [17] for dynamical pattern recognition.

III. EXPERIMENTAL FLOW PATTERN ANALYSIS BASED ON NETWORK MOTIF DISTRIBUTION

A. Inclined oil-water two-phase flow experiment

The inclined oil-water two-phase flow experiment in a 125-mm-diameter pipe was carried out in the multiphase flow loop laboratory in Tianjin University. The measurement system consists of several parts: a vertical multielectrode array (VMEA) conductance sensor (Fig. 4) that was specifically designed for the two-phase flow experiment [48], miniconductance probes, signal generating circuit, signal modulating module, data acquisition device (PXI 4472 card, National Instruments), and signal analysis software. The measurement system uses a 20 kHz constant voltage (1.4 V) sinusoidal wave to excite the flow. The signal modulating module consists of three submodules: differential amplifier, sensitive demodulation, and low-pass filter. The data processing part is realized through graphical programming language LABVIEW 7.1 embedded in the data acquisition card, which can display, store, and analyze data wave forms in real time.

Experiments were performed by initially introducing both water and oil flows into the pipe. The water flow rate was fixed and oil flow rate was gradually increased. Each time when the ratio between the oil and water flow rates reached a certain preset value, conductance fluctuating signals were acquired from the VMEA sensor. In our experiment, the inclined angle was set to 45° and the water phase flow rate was between 0.0057 and 0.3306 m/s and the oil phase rate was from 0.0052 to 0.3306 m/s. The sampling frequency was 400 Hz and the sampling data recording time for one measuring point was 60 s. Based on the flow pattern definition proposed by Flores *et al.* [3], we have observed three different inclined oil-water two-phase flow patterns in the experiment, as shown in Fig. 5, i.e., CT, PS, and transitional flow patterns.

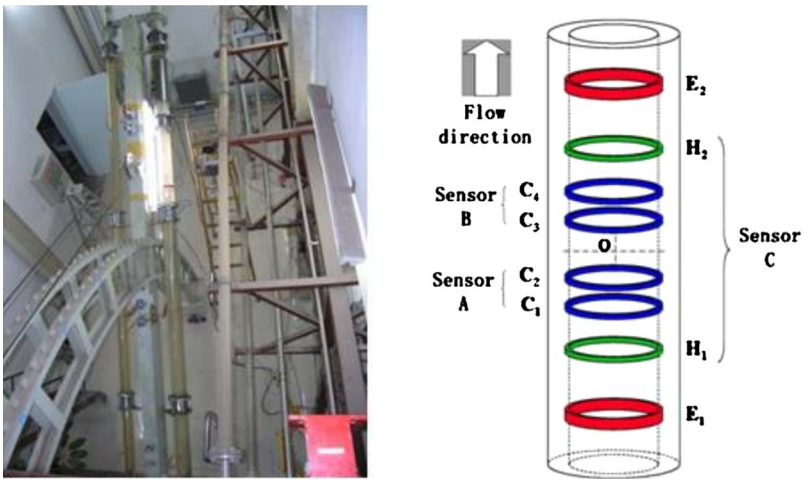

FIG. 4. (Color online) Experimental flow loop facility and VMEA conductance sensor.

FIG. 5. Experimentally observed flow patterns: from left to right are PS, CT, and TF, respectively.

The conductance fluctuating signals corresponding to the three flow patterns are shown in Fig. 6, where U_{so} and U_{sw} represent oil superficial velocity and water superficial velocity, respectively.

B. Two-phase flow PSCN and motif distribution

Figure 7 shows the PSCNs associated with the three distinct types of two-phase flow patterns. The respective motif distributions are shown in Fig. 8. We observe a common feature among the distributions: heterogeneity. The similarity to the motif distributions from typical chaotic systems leads us to speculate that the dynamics underlying the three flow patterns may be chaotic. While the observed motif distributions all appear heterogeneous, the degrees of heterogeneity are apparently different for different flow patterns, where the transitional flow exhibits the most heterogeneous distribution. To give credence to our proposition that the dynamics of two-phase flows are chaotic, we have computed the maximal Lyapunov exponent (MLE) from time series by using a standard method [49]. The MLE is computed by abandoning the first 1000 transient data points and using the following 10 000 data points. The estimate MLEs are 0.084 ± 0.008, 0.055 ± 0.003, and 0.037 ± 0.003 for TF, CT, and PS flows, respectively. All MLEs are positive, suggesting strongly the chaotic nature of the underlying flows. More remarkably, the flow with the largest value of MLE corresponds to the most heterogeneous PSCN motif distribution.

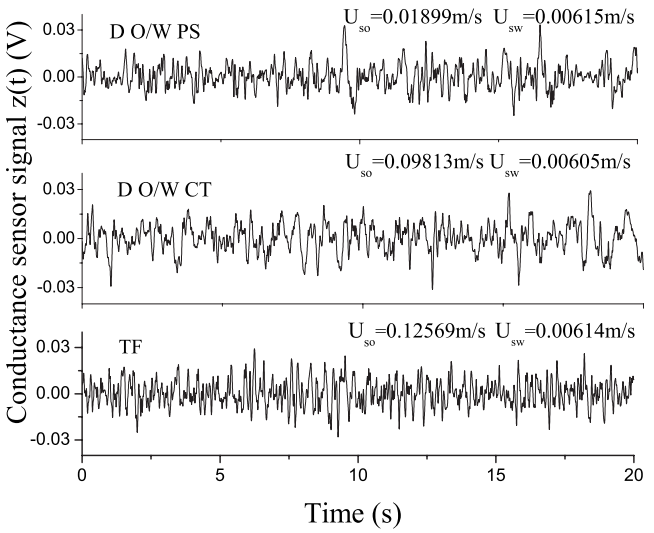

FIG. 6. Conductance fluctuating signals corresponding to PS, CT, and TF patterns.

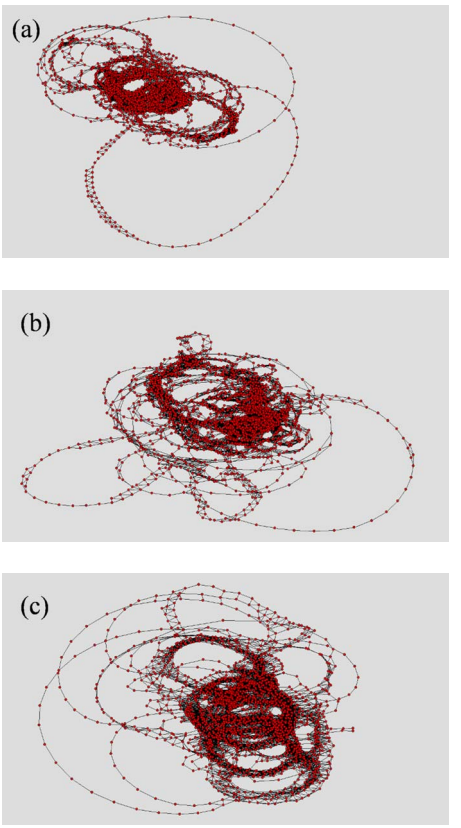

FIG. 7. (Color online) PSCNs associated with three distinct types of two-phase flow patterns: (a) PS flow (U_{so} =0.018 99 m/s, U_{sw}=0.006 15 m/s), (b) CT flow (U_{so} =0.098 13 m/s, U_{sw}=0.006 05 m/s), and (c) transitional flow (U_{so}=0.125 69 m/s, U_{sw}=0.006 14 m/s). Each network is constructed by setting threshold r_c to be 20% of the rms value of the measured conductance fluctuating signal and contains 2000 nodes.

PS flow occurs at slightly higher superficial water velocities than those for CT flows. For low to moderate superficial oil velocities, the sequence of oil droplets originally observed in CT flow patterns is interrupted by water breaks, with the oil droplets grouping closer and forming packs at

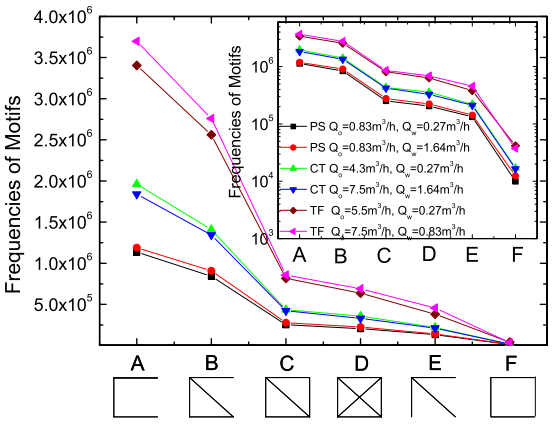

FIG. 8. (Color online) PSCN motif distributions of three distinct flow patterns (two signals for each flow pattern). The inset shows the motif distributions in logarithmic scale.

the top of the pipe (see Fig. 5). Due to the approximately periodic switch between oil-plug and water-plug movements, the flow also exhibits approximately regular dynamics to some extent, leading to the smallest MLE value and, consequently, to the weakest heterogeneity in the motif distribution as characterized by, e.g., low frequencies of occurrences of motifs A and B as compared with those of the CT and transitional flows.

CT flows appear for low to moderate superficial oil and water velocities. In this flow pattern, oil disperses in the continuous water in the form of discrete well rounded droplets of mostly small to medium size (see Fig. 5). Because of the density difference between oil and water, the droplets pass the upper regions of the pipe in an uninterrupted sequence with nearly uniform vertical spread. The prominent characteristic of CT flow patterns is the local countercurrent flow of water, which usually occurs at the bottom side of the pipe. The countercurrent phenomenon is due to the increasing magnitude of the gravitational component in the direction opposite to the main flow, which partially overcomes the linear momentum of the water phase. Reflected in the motif distribution, we observed that the frequencies of motifs A and B increase as the flow pattern evolves from PS to CT. Indeed, we find that the values of MLE for CT flows tend to be larger than those for PS flows.

Transitional flows arise at moderate oil superficial velocities associated with low to moderate superficial water velocities, which appear in the regime between the water-dominated and oil-dominated flow patterns. In the TF regime, oil regions form at the top side of the pipe, while water exists at the bottom of the pipe with a few recirculating oil droplets. In the middle region the oil and water phases appear alternatively as a continual phase (Fig. 5). TF patterns thus appear more complex than PS and CT flows. Indeed, we find that the values of the MLE associated with transitional flows are generally larger. As can be seen from Fig. 8, the motif distributions associated with the TFs are more heterogeneous than those with PS and CT flows.

We now provide the motivation for our network-characterization method by comparing with the approach proposed in Ref. [17], in which a fixed number of nearest neighbors are selected for defining connections for each phase-space node. In this scheme, different dynamical families can be distinguished by the subgraph distributions. In each family, e.g., a chaotic family, the subgraph distributions of different chaotic systems overlap but the distributions differ among distinct families. Although the approach is effective for different types of dynamics, there is a need to develop an alternative method to identify different dynamical systems belonging to the same class, which can then be applied to experimental two-phase flows exhibiting similar chaotic features (e.g., with approximately the same MLEs). This consideration motivates us to exploit network-construction methods based on the distances among points (nodes) in the phase space and motif distributions. The heterogeneity present in the distributions for three types of flow patterns demonstrates the effectiveness of our method in characterizing complex dynamics associated with two-phase flows.

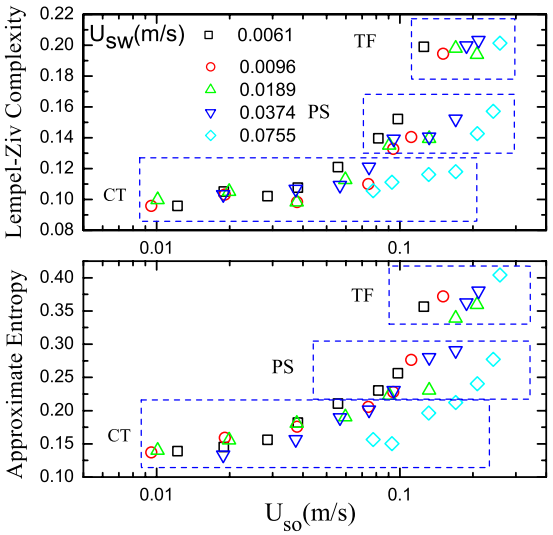

FIG. 9. (Color online) Dependence of (top) Lempel-Ziv complexity and (bottom) approximate entropy on the oil superficial velocity U_{so} under different water superficial velocities U_{wo} for three flow patterns TF, PS, and CT.

IV. COMPLEXITY MEASURES

We investigate complexity measures to provide further support for the effectiveness our motif-distribution-based method in characterizing and distinguishing different flow patterns. In particular, we use two measures: Lempel-Ziv complexity and approximate entropy.

The Lempel-Ziv complexity was proposed for characterizing stochastic time series [50,51]. Briefly, the measure tends to unity for completely random sequences and zero for regular and periodic signals (for details, see Refs. [50,51]). The approximate entropy is a "regularity statistic" that quantifies the unpredictability of fluctuations in a time series. Intuitively, it can be expected that the presence of repetitive patterns of fluctuation in a time series renders it more predictable than a time series in which such patterns are absent. The approximate entropy reflects the likelihood that "similar" patterns of observations will be followed by additional similar observations. The more repetitive patterns a time series contains, the smaller is the value of the approximate entropy. The approximate entropy can be computed by following the processes detailed in Ref. [52].

Figure 9 shows the Lempel-Ziv complexity and the approximate entropy calculated from 39 conductance fluctuating signals of three flow patterns versus the oil superficial velocity U_{so} for different values of water superficial velocity U_{wo}. It demonstrates that TF flows possess the highest degree of complexity while PS flows have the lowest value, with values from the CT flows lying in between, providing support for our results based on motif distributions in that more heterogeneous distributions indicate behaviors associated with higher values of the complexity measures.

V. CONCLUSIONS

Despite tremendous knowledge about fluid flows, our understanding of two-phase flows is still quite limited. We have

proposed a scheme based on network motifs to characterize and distinguish three typical two-phase patterns observed in water-oil flow experiment. Given a measured time series from a flow pattern, our idea is to construct a phase space and then a network based on a distance metric, and examine the frequency distribution of a number of network motifs. The method is first validated by using classical chaotic systems and then applied to experimental two-phase flow patterns. We find that the three most commonly occurring patterns in two-phase flows all exhibit heterogeneous motif distributions, mimicking those from chaotic systems. More remarkably, the degrees of the heterogeneity in the distribution are distinctly different for the three types of flow patterns, consistent with the Lyapunov-exponent estimates. We have also computed two measures of complexity, Lempel-Ziv complexity and approximate entropy, for the three types of flow patterns and observed that flows with more heterogeneous motif distributions tend to have higher complexity measures. These results suggest the power of network motifs to characterize and distinguish complex flow patterns.

The last decade has witnessed a tremendous growth in the study of complex networks, and network-based theories and methodologies have been increasingly applied to addressing fundamental problems in many disciplines. Understanding of inclined oil-water two-phase flows as a class of complex nonlinear dynamical systems has remained to be poor. By introducing the complex-network idea and proposing the method of network motif distribution, we have obtained other insights into the dynamics of two-phase flows, particularly in terms of the transition from one pattern to another. Network motifs have been a powerful tool in analyzing network dynamics in other disciplines such as systems biology [32], and we hope that the approach can also be useful for other complex systems in science and engineering.

ACKNOWLEDGMENTS

Z.K.G. and N.D.J. were supported by the National Natural Science Foundation of China (Grant No. 50974095) and the National High Technology Research and Development Program of China (Grant No. 2007AA06Z231). W.X.W. and Y.C.L. were supported by AFOSR under Grant No. FA9550-09-1-0260.

[1] A. D. Hill and T. Oolman, JPT, J. Pet. Technol. **34**, 2432 (1982).
[2] P. Vigneaux, P. Chenais, and J. P. Hulin, AIChE J. **34**, 781 (1988).
[3] J. G. Flores, X. T. Chen, C. Sarica, and J. P. Brill, SPE Prod. Facil. **14**, 102 (1999).
[4] S. D. Mobbs and G. P. Lucas, Appl. Sci. Res. **51**, 263 (1993).
[5] G. P. Lucas, Chem. Eng. J. **56**, 167 (1995).
[6] G. P. Lucas and N. D. Jin, Meas. Sci. Technol. **12**, 1546 (2001).
[7] G. P. Lucas and N. D. Jin, Meas. Sci. Technol. **12**, 1529 (2001).
[8] H. Kantz and T. Schreiber, *Nonlinear Time Series Analysis* (Cambridge University Press, Cambridge, UK, 1997).
[9] Y. B. Zong, N. D. Jin, Z. Y. Wang, Z. K. Gao, and C. Wang, Int. J. Multiphase Flow **36**, 166 (2010).
[10] J. P. Eckmann, S. O. Kamphorst, and D. Ruelle, EPL **4**, 973 (1987).
[11] N. Marwan, N. Wessel, U. Meyerfeldt, A. Schirdewan, and J. Kurths, Phys. Rev. E **66**, 026702 (2002).
[12] M. Annunziato and H. D. I. Abarbanel, Proceedings of International Conference on Soft Computing, SOCO, Genova, Italy, 1999 (unpublished).
[13] Z. K. Gao and N. D. Jin, Phys. Rev. E **79**, 066303 (2009).
[14] J. Zhang and M. Small, Phys. Rev. Lett. **96**, 238701 (2006).
[15] Y. Yang and H. J. Yang, Physica A **387**, 1381 (2008).
[16] L. Lacasa, B. Luque, F. Ballesteros, J. Luque, and J. C. Nuno, Proc. Natl. Acad. Sci. U.S.A. **105**, 4972 (2008).
[17] X. Xu, J. Zhang, and M. Small, Proc. Natl. Acad. Sci. U.S.A. **105**, 19601 (2008).
[18] J. Zhang, J. Sun, X. Luo, K. Zhang, T. Nakamura, and M. Small, Physica D **237**, 2856 (2008).
[19] Y. Shimada, T. Kimura, and T. Ikeguchi, Lect. Notes Comput. Sci. **5163**, 61 (2008).
[20] R. V. Donner, Y. Zou, J. F. Donges, N. Marwan, and J. Kurths, New J. Phys. **12**, 033025 (2010).
[21] R. V. Donner, Y. Zou, J. F. Donges, N. Marwan, and J. Kurths, Phys. Rev. E **81**, 015101(R) (2010).
[22] D. J. Watts and S. H. Strogatz, Nature (London) **393**, 440 (1998).
[23] A. L. Barabási and R. Albert, Science **286**, 509 (1999).
[24] R. Albert and A.-L. Barabási, Rev. Mod. Phys. **74**, 47 (2002).
[25] M. E. J. Newman, SIAM Rev. **45**, 167 (2003).
[26] S. N. Dorogovtsev and J. F. F. Mendes, Adv. Phys. **51**, 1079 (2002).
[27] W.-X. Wang, B.-H. Wang, B. Hu, G. Yan, and Q. Ou, Phys. Rev. Lett. **94**, 188702 (2005).
[28] R. Yang, W.-X. Wang, Y.-C. Lai, and G.-R. Chen, Phys. Rev. E **79**, 026112 (2009).
[29] J. Ren, W.-X. Wang, B.-W. Li, and Y.-C. Lai, Phys. Rev. Lett. **104**, 058701 (2010).
[30] R. Milo, S. ShenOrr, S. Itzkovitz, N. Kashan, D. Chklovskii, and U. Alon, Science **298**, 824 (2002).
[31] R. Milo, S. Itzkovitz, N. Kashtan, R. Levitt, S. ShenOrr, I. Ayzenshtat, M. Sheffer, and U. Alon, Science **303**, 1538 (2004).
[32] U. Alon, *An Introduction to Systems Biology—Design Principles of Biological Circuits* (Chapman & Hall/CRC, Boca Raton, FL, 2007).
[33] A. Vazquez, R. Dobrin, D. Sergi, J. P. Eckmann, Z. N. Oltvai, and A. L. Barabási, Proc. Natl. Acad. Sci. U.S.A. **101**, 17940 (2004).
[34] K. Baskerville, P. Grassberger, and M. Paczuski, Phys. Rev. E **76**, 036107 (2007).
[35] Z. K. Gao and N. D. Jin, Chaos **19**, 033137 (2009).
[36] F. Takens, in *Dynamical Systems and Turbulence*, edited by D.

A. Rand and L.-S. Young (Springer-Verlag, Berlin, 1980).
[37] N. H. Packard, J. P. Crutchfield, J. D. Farmer, and R. S. Shaw, Phys. Rev. Lett. **45**, 712 (1980).
[38] T. Sauer, J. A. Yorke, and M. Casdagli, J. Stat. Phys. **65**, 579 (1991).
[39] H. S. Kim, R. Eykholt, and J. D. Salas, Physica D **127**, 48 (1999).
[40] M. B. Kennel, R. Brown, and H. D. I. Abarbanel, Phys. Rev. A **45**, 3403 (1992).
[41] E. N. Lorenz, J. Atmos. Sci. **20**, 130 (1963).
[42] O. E. Rössler, Phys. Lett. **57**, 397 (1976).
[43] T. Kamada and S. Kawai, Inf. Process. Lett. **31**, 7 (1989).
[44] S. Wernicke and F. Rasche, Bioinformatics **22**, 1152 (2006).
[45] S. Wernicke, IEEE/ACM Trans. Comput. Biol. Bioinf. **3**, 347 (2006).
[46] S. P. Borgatti, M. G. Everett, and L. C. Freeman, *UCINET for Windows: Software for Social Network Analysis* (Analytic Technologies, Harvard, MA, 2002).
[47] W. Nooy, A. Mrvar, and V. Batagelj, *Exploratory Social Network Analysis with PAJEK* (Cambridge University Press, New York, 2005).
[48] N. D. Jin *et al.*, Meas. Sci. Technol. **19**, 045403 (2008).
[49] A. Wolf, J. B. Swift, H. L. Swinney, and J. A. Vastano, Physica D **16**, 285 (1985).
[50] A. Lempel and J. Ziv, IEEE Trans. Inf. Theory **22**, 75 (1976).
[51] F. Kaspar and H. G. Schuster, Phys. Rev. A **36**, 842 (1987).
[52] S. M. Pincus, Proc. Natl. Acad. Sci. U.S.A. **88**, 2297 (1991).